ChemPubSoc Europe

DOI: 10.1002/cphc.201500514

CHEMPHYSCHEM Articles

Understanding J-Modulation during Spatial Encoding for Sensitivity-Optimized Ultrafast NMR Spectroscopy

Boris Gouilleux,[a] Laetitia Rouger,[a] Benoît Charrier,[a] Ilya Kuprov,[b] Serge Akoka,[a] Jean-Nicolas Dumez,*[c] and Patrick Giraudeau*[a, d]

Ultrafast (UF) NMR spectroscopy is an approach that yields 2D spectra in a single scan. This methodology has become a powerful analytical tool that is used in a large array of applications. However, UF NMR spectroscopy still suffers from an intrinsic low sensitivity, and from the need to compromise between sensitivity, spectral width, and resolution. In particular, the modulation of signal intensities by the spin–spin *J*-coupling interaction (J-modulation) impacts significantly on the intensities of the spectral peaks. This effect can lead to large sensitivity losses and even to missing spectral peaks, depending on the nature of the spin system. Herein, a general simulation package (Spinach) is used to describe J-modulation effects in UF experiments. The results from simulations match with experimental data and the results of product operator calculations. Several methods are proposed to optimize the sensitivity in UF COSY spectra. The potential and drawbacks of the different strategies are also discussed. These approaches provide a way to adjust the sensitivity of UF experiments for a large range of applications.

1. Introduction

Two-dimensional (2D) NMR spectroscopy is a powerful analytical tool used in a wide array of applications such as structure elucidation, quantitative analysis, or metabolomics.[1] Conventional 2D NMR spectroscopy experiments suffer from an intrinsic long experiment duration, which is necessary to obtain the indirect dimension by repeating numerous transients with incremented delays. This long acquisition duration makes conventional 2D NMR spectroscopy sensitive to hardware instabilities in the course of the experiment, and is unsuitable for the study of fast processes or coupling with other techniques.[2] A large number of methods have been proposed to cope with this time limitation. Some of these approaches consist of optimizing recovery delays and pulse angles, such as the SOFAST,[3] BEST,[4] or ASAP[5] approaches. Several other strategies have been developed to improve the length of 2D experiments by reducing the number of t_1 increments; subsequent resolution losses are compensated for by adapted signal processing methods.[6] Others are based on an alternative to Fourier transform (FT) NMR spectroscopy, such as Hadamard spectroscopy.[7] A decade ago, Frydman and co-workers developed a new generic multidimensional approach, ultrafast (UF) NMR spectroscopy, to yield homo- or heteronuclear 2D spectra in a single scan.[8] With this method, the incrementation of the evolution period t_1 is replaced by a spatial encoding scheme. After a conventional mixing period, the spatially encoded information is decoded by a detection block based on echo planar spectroscopic imaging (EPSI).[9] At the heart of this methodology, the spatial encoding step is generally performed in a continuous fashion thanks to a combination of bipolar gradients and linearly frequency-swept pulses.[10] In particular, the phase-modulated encoding block, which uses a double spin echo scheme, has been established as the optimum compromise between sensitivity and resolution.[11]

Because its performance has been significantly improved during the last decade, UF NMR spectroscopy is now an efficient method that is applied in numerous fields, such as metabolomics; real-time reaction monitoring; or hybrid techniques, such as chromatography and dissolution dynamic nuclear polarization (DNP).[12] However, in spite of its high potential, this approach still suffers from an intrinsic low sensitivity and from the need to compromise between sensitivity, spectral width, and resolution,[13] even if several strategies have been proposed to alleviate this compromise.[14] There are several reasons for these sensitivity losses, such as the need to record the signal in the presence of strong gradients, leading to large digital filter bandwidths that have an impact on the signal-to-noise ratio (SNR) or the effect of translational molecular diffusion during spatial encoding.[15]

A significant source of sensitivity losses in UF NMR spectroscopy is the effect of spin–spin scalar couplings (*J*-couplings) during the spatial encoding step. Because most UF experi-

[a] B. Gouilleux, L. Rouger, B. Charrier, Prof. S. Akoka, Dr. P. Giraudeau
CEISAM CNRS, UMR6230, Université de Nantes, BP 92208
2 rue de la Houssinière, 44322 Nantes (France)
E-mail: patrick.giraudeau@univ-nantes.fr

[b] Dr. I. Kuprov
School of Chemistry, University of Southampton
University Road, Southampton SO17 1BJ (UK)

[c] Dr. J.-N. Dumez
CNRS UPR2301, Institut de Chimie des Substances Naturelles
1 avenue de la Terrasse, 91198 Gif-sur-Yvette Cedex (France)
E-mail: jeannicolas.dumez@cnrs.fr

[d] Dr. P. Giraudeau
Institut Universitaire de France, 1 rue Descartes
75005, Paris Cedex 05 (France)

ments rely on an encoding step, in which all spins spend an equal amount of time in the transverse plane—a "constant-time" (CT) approach—the intensity of the detected signals is modulated by *J*-couplings in a complex, spin-system-dependent way. This J-modulation effect is well described in the case of conventional CT experiments,[16] but remains poorly understood for UF experiments that rely on spatial encoding. Because J-modulation can lead to large SNR losses, and even to missing spectral peaks, there is a motivation to develop tools for its understanding and control, which may result in ways to optimize the SNR of UF experiments. We propose herein a description of J-modulation effects in a large range of spin systems to predict their impact on sensitivity. Thus, we first rely on a theoretical description, then on numerical simulations for more complicated spin systems with strong couplings. The calculated J-modulation effects are also compared with experimental results, and finally used to optimize the sensitivity in a variety of situations.

2. Theory

2.1. Pulse Sequence

To evaluate the impact of J-modulation on the signal of CT UF experiments, in this section we introduce a theoretical description that uses the product operator formalism. We focus herein on the case of UF CT-COSY, which is one of the most widely used UF experiments that relies on a CT phase-modulated spatial encoding. This double spin echo method starts with a hard 90° pulse, followed by the application of a pair of 180° chirp pulses applied during alternating gradients (Figure 1 A). The CT nature of this scheme is due to the identical time spent in the transverse plane by all spins regardless of their position along the *z* axis. A theoretical description of this pulse sequence applied to a system of two coupled spins has been already proposed by Wu et al.,[17] who established an expression for the density matrix at the beginning of detection, which showed a J-modulation that was different for the diagonal peak (cosine modulation) and cross-peak (sine modulation). It is also demonstrated that this modulation depends on the scalar coupling constant, *J*, and on the total time, *T*, spent in the transverse plane. In practice, this J-modulation can be modified by adding a new delay called t_{mix} prior to the spatial encoding step, which allows the total time spent by the spins in the transverse plane to be controlled (Figure 1 A). Given the trigonometric nature of the J-modulation, there is an optimal t_{mix} value, which maximizes the sensitivity, depending on the spin system and coupling constant. Because J-modulation effects in more complex spin systems were not described by Wu et al., it was necessary to extend this initial description to a more general $A_NM_PX_Q$ system.

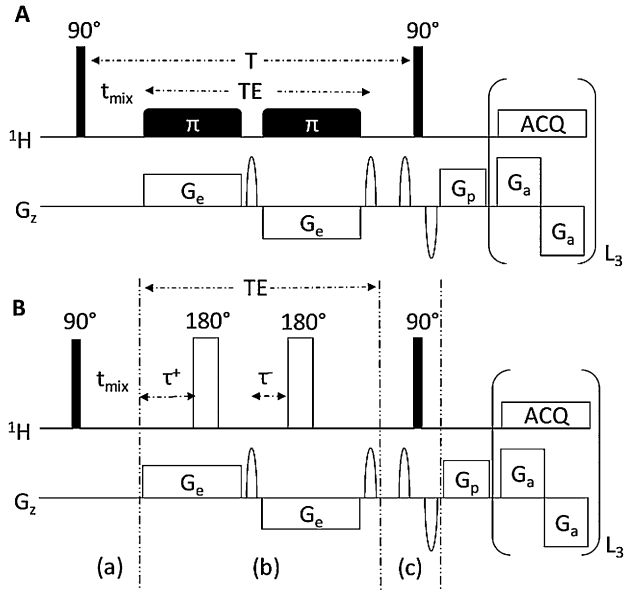

Figure 1. Pulse sequence of UF CT-COSY (A) and a schematic view under the assumption of instantaneous inversion (B). *TE* = duration of spatial coding, ACQ = acquisition.

2.2. Spin System and Interactions

Consider three coupled spins $^1/_2$:A, M, and X. The propagation of the density matrix is computed with the product operator formalism, ignoring relaxation and diffusion effects. Only the case of weak couplings is considered with analytical calculations; strong couplings are treated numerically. In the case of weak couplings, the free precession Hamiltonian (*H*) for an $A_NM_PX_Q$ system is expressed by Equation (1):

$$H = \sum_n \Omega_A A_{nz} + \sum_p \Omega_M M_{pz} + \sum_q \Omega_X X_{qz} + 2\pi J_{AM} \sum_n \sum_p A_{nz} M_{pz} + 2\pi J_{AX} \sum_n \sum_q A_{nz} X_{qz} + 2\pi J_{MX} \sum_p \sum_q M_{pz} X_{qz} \quad (1)$$

in which Ω_i is the chemical shift offset of spin *i*, and J_{ij} is the scalar coupling constant between spins *i* and *j*. An important feature is the response of the spins to the π-chirp pulses during spatial encoding with alternating excitation gradients $\pm Ge$. The proposed description assumes an instantaneous rotation provided by the chirp pulse (Figure 1 B), if its carrier pulsation, $O^{(\tau)}$, matches the total offset of the spin *i*: $O^{(\tau)} = \Omega_i \pm \gamma Gez$. This is a common assumption already proposed by Tal and Frydman.[9b]

The last point to be considered is the different rotation time of the spins included in the same spin system. As shown in the previous matching equation, for a given slice *z*, the carrier frequency of the chirp does not match the different total offsets of each spin simultaneously. This results in small additional delays in the predicted modulation. Numerical simulations show, however, that these delays can be reasonably neglected under typical experimental parameters. Therefore, they are not considered further.

2.3. Density Matrix Propagation

Consider the application of the UF CT-COSY pulse sequence to a general $A_NM_PX_Q$ spin system. The effective length of the sample is L and the z coordinate ranges from $-L/2$ to $L/2$. All radiofrequency (RF) pulses are applied along the x axis and the density matrix is propagated under the assumptions discussed previously. The initial density matrix is given by Equation (2):

$$\sigma_{[0]} = \boldsymbol{A}_{1z} \tag{2}$$

After the first 90° pulse, the matrix is given by Equation (3):

$$\sigma_{[0^+]} = -\boldsymbol{A}_{1y} = -\frac{1}{2i}(\boldsymbol{A}_{1+} - \boldsymbol{A}_{1-}) \tag{3}$$

Given the coherence transfer pathway (CTP) {0, −1, +1, −1, −1} only the evolution of $\boldsymbol{A}_{1-}$ is relevant. During period a (Figure 1 B), the density matrix evolves with the free precession Hamiltonian for a duration of t_{mix} [Eq. (4)]:

$$\sigma_{[0^+]} \xrightarrow{H_{FP} t_{mix}} \sigma_{[\alpha]} =$$
$$\frac{1}{2i}\begin{Bmatrix} \cos(\pi J_{AM} t_{mix})^P \cos(\pi J_{AX} t_{mix})^Q \boldsymbol{A}_{1-} \\ i\cos(\pi J_{AX} t_{mix})^Q \cos(\pi J_{AM} t_{mix})^{P-1} \sin(\pi J_{AM} t_{mix}) \sum_p 2\boldsymbol{A}_{1-}\boldsymbol{M}_{pz} \\ i\cos(\pi J_{AM} t_{mix})^P \cos(\pi J_{AX} t_{mix})^{Q-1} \sin(\pi J_{AX} t_{mix}) \sum_q 2\boldsymbol{A}_{1-}\boldsymbol{X}_{qz} \end{Bmatrix} e^{i\Omega_A t_{mix}} \tag{4}$$

Here only operators providing a signal during detection are retained; in particular, operators in "multiple antiphase" are ignored because none of them provide in phase −1 order operators. Then spatial encoding generates a phase depending on the z position as given by Equation (5):

$$\sigma_{[b]} =$$
$$\frac{1}{2i}\begin{Bmatrix} \cos(\pi J_{AM} T)^P \cos(\pi J_{AX} T)^Q \boldsymbol{A}_{1-} \\ i\cos(\pi J_{AX} T)^Q \cos(\pi J_{AM} T)^{P-1} \sin(\pi J_{AM} T) \sum_p 2\boldsymbol{A}_{1-}\boldsymbol{M}_{pz} \\ i\cos(\pi J_{AM} T)^P \cos(\pi J_{AX} T)^{Q-1} \sin(\pi J_{AX} T) \sum_q 2\boldsymbol{A}_{1-}\boldsymbol{X}_{qz} \end{Bmatrix} e^{i\Omega_A t_{mix}} e^{iC\Omega_A z} \tag{5}$$

in which C refers to the spatiotemporal encoding constant ($C = 2TE/L$). After the mixing period, that is, the action of the second hard 90° pulse, the coherence transfer is obtained from Equation (6):

$$\sigma_{[c]} =$$
$$\frac{1}{4i}\begin{Bmatrix} \cos(\pi J_{AM} T)^P \cos(\pi J_{AX} T)^Q \boldsymbol{A}_{1-} \\ -\cos(\pi J_{AX} T)^Q \cos(\pi J_{AM} T)^{P-1} \sin(\pi J_{AM} T) \sum_p 2\boldsymbol{A}_{1z}\boldsymbol{M}_{p-} \\ -\cos(\pi J_{AM} T)^P \cos(\pi J_{AX} T)^{Q-1} \sin(\pi J_{AX} T) \sum_q 2\boldsymbol{A}_{1z}\boldsymbol{X}_{q-} \end{Bmatrix} e^{i\Omega_A t_{mix}} e^{iC\Omega_A z} \tag{6}$$

Thanks to the density matrix established at the beginning of detection, that is, $t_2 = 0$, the analytical expressions of J-modulation of the diagonal peak S_{AA} and of the cross-peaks S_{AM} and S_{AX} are obtained from Equation (7):

$$\begin{aligned} S_{AA} &\propto \cos(\pi J_{AM} T)^P \cos(\pi J_{AX} T)^Q \\ S_{AM} &\propto \cos(\pi J_{AX} T)^Q \cos(\pi J_{AM} T)^{P-1} \sin(\pi J_{AM} T) \\ S_{AX} &\propto \cos(\pi J_{AM} T)^P \cos(\pi J_{AX} T)^{Q-1} \sin(\pi J_{AX} T) \end{aligned} \tag{7}$$

These expressions show how J-modulation depends on the scalar coupling constants and on the total time, T, spent in the transverse plane, which has an impact in a variety of ways on the peak intensities. This total time may be tuned by varying the t_{mix} delay placed immediately after excitation.

Computational Details

Numerical Simulations

Numerical simulations were performed by using the Fokker–Planck theory module implemented in version 2.0 of Spinach library.[18] The calculation was performed in the direct product $\boldsymbol{F}$ of spin-state space $\boldsymbol{S}$ and the three-dimensional Cartesian space $\boldsymbol{R}^3$ [Eq. (8)]:

$$\boldsymbol{F} = \boldsymbol{S} \otimes \boldsymbol{R}^3 \tag{8}$$

Matrix representations of the spin Hamiltonian $\boldsymbol{H}$, the diffusion operator $\boldsymbol{D}$, and the magnetic-field gradient operators $\{\boldsymbol{G}_x, \boldsymbol{G}_y, \boldsymbol{G}_z\}$ have the expressions given in Equation (9) in the Fokker–Planck space:

$$\begin{aligned} &\boldsymbol{H}(t) = \hat{\hat{H}}(t) \otimes \boldsymbol{1} \quad \boldsymbol{D} = D\left(\boldsymbol{1} \otimes \left[\frac{\partial^2}{\partial x^2} + \frac{\partial^2}{\partial y^2} + \frac{\partial^2}{\partial z^2}\right]\right) \\ &\boldsymbol{G}_x = \hat{\hat{L}}_\gamma \otimes x \quad \boldsymbol{G}_y = \hat{\hat{L}}_\gamma \otimes y \quad \boldsymbol{G}_z = \hat{\hat{L}}_\gamma \otimes z \quad \hat{\hat{L}}_\gamma = \sum_k \gamma_k \hat{\hat{L}}_z^{(k)} \end{aligned} \tag{9}$$

in which D is the diffusion coefficient, $\boldsymbol{1}$ is a unit matrix of an appropriate dimension, $\hat{\hat{H}}(t)$ is the spin Hamiltonian commutation superoperator, γ_k are magnetogyric ratios of the spins in the system, and $\hat{\hat{L}}_z^{(k)}$ are the corresponding longitudinal spin commutation superoperators. Finite-difference matrices[19] were used as representations of the differentiation operators. The resulting equation of motion given by Equation (10):

$$\begin{aligned} &\boldsymbol{F}(t) = \boldsymbol{H}(t) + g_x(t)\boldsymbol{G}_x + g_y(t)\boldsymbol{G}_y + g_z(t)\boldsymbol{G}_z + i\boldsymbol{D} \\ &\frac{d}{dt}\boldsymbol{\rho}(t) = -i\boldsymbol{F}(t)\boldsymbol{\rho}(t) \end{aligned} \tag{10}$$

in which $g_{x,y,z}$ are gradient amplitudes, was solved for the free induction decay, $f(t)$, by using the standard time-ordered exponential propagation technique[20] with the initial condition $\boldsymbol{\rho}_0$ set to spatially uniform longitudinal magnetization and the detection state $\boldsymbol{\sigma}$ to spatially uniform $\hat{L}_+$ spin operator [Eq. (11)]:

$$f(t) = \left\langle \boldsymbol{\sigma} \middle| \exp_{(o)}\left(-i\int_0^t \boldsymbol{F}(t)dt\right) \middle| \boldsymbol{\rho} \right\rangle \tag{11}$$

The trajectory-level state space restriction functionality of Spinach[21] was used to keep matrix dimensions manageable throughout the simulation. The number of points in the discretization of $\boldsymbol{R}^3$ and the finite difference stencil size were increased until convergence was achieved in the simulation result.

All simulated spectra were obtained with the following features. Acquisition parameters: 512 points separated by a dwell time of 0.55 μs were used to compute the UF dimension, whereas the conventional one was obtained with 128 loops in the detection block.

Acquisition gradients were fixed at 0.687 T m^{-1}. For the encoding parameters, excitation gradients of 0.020 T m^{-1} were applied, whereas the π-chirp pulses were performed by a WURST built with 1000 points, sweeping a bandwidth of 13 kHz in 15 ms. The second chirp of the double spin echo was flanked by two crushers. The CTP was completed in the same way as that shown in Figure 1 A, through gradient pulses at 0.48 T m^{-1} applied for 1 ms.

The length of the sample was fixed at 1.5 cm and the simulation was performed with 500 grid points in the *z* direction. In all simulations, a B_0 field of 11.77 T m^{-1} was considered and ideal pulses were assumed. The simulated 2D FID was then processed in the same way as the experimental spectra: sinusoidal apodization for the conventional dimension and a Gaussian apodization was applied in the UF dimension, including zero filling in both dimensions.

Sample Preparation

The experimental UF CT-COSY spectrum of histidine (His; Figure 3 F, below) was recorded on a sample containing His dissolved in a mixture of phosphate buffer (pH 7) and D_2O (1 mL; 37.5/62.5 v/v) to obtain a concentration of 110 mmol L^{-1}. The UF CT-COSY spectra related to Figures 2 B and 3 E below were recorded on samples of alanine (Ala) at 100 mmol L^{-1} and taurine (Tau) at 160 mmol L^{-1}, respectively, in D_2O. The metabolic mixture related to Figure 4 B and C, below, was prepared with four metabolites: Ala, lactate (Lac), threonine (Thr), and Tau, plus choline (Cho) acting as an internal relaxation reference, dissolved in a mixture of phosphate buffer (pH 7) and D_2O (2.4 mL; 37.5/62.5 v/v), leading to a concentration of 50 mmol L^{-1} for each metabolite.

The UF CT-COSY spectra related to Figure 5 C, D, and G, below, were recorded on a 207 mmol L^{-1} ferulic acid sample in [D_6]acetone.

NMR Spectrometry

NMR spectra were recorded at 298 K on a Bruker Avance III 500 spectrometer, operating at a proton frequency of 500.13 MHz and equipped with a dual ^{1}H/^{13}C cryogenic probe, including a *z*-axis gradient. Conventional 1D experiments were recorded with routine pulse sequences available within the commercial software Bruker Topspin 2.1.

UF Experiments

For all UF experiments, spatial encoding was performed by using a CT spatial encoding scheme, that is, double spin echo with 15 ms smoothed chirp encoding pulses. The sweep range for the encoding pulses was set to 13 kHz for all spectra, and the amplitude of the encoding gradients was adapted to obtain a frequency dispersion equivalent to the frequency range of the pulses: $Ge = 0.0204$ T m^{-1}. Coherence-selection gradients were added for the UF CT-COSY, as indicated in Figure 1 A. The acquisition gradient parameters were set as follows: 0.688 T m^{-1} for the sample of Tau, His, and metabolic mixture; 0.573 T m^{-1} for experiments on the sample of ferulic acid. For all experiments, the acquisition gradient duration was $Ta = 281.6$ μs and the detecting block used 128 detection gradients pairs. Specific processing of the UF spectra was performed with MATLAB by using the same method as that described for the simulated spectra.

3. Results and Discussion

We discuss herein the ability to predict J-modulation effects with both numerical simulations and analytical expressions. Several spin systems are considered, including different regimes of scalar couplings, that is, weak and strong couplings, through comparisons between computed J-modulation and experimental results. Calculations of J-modulation are used to customize the UF CT-COSY experiments and improve its sensitivity in a variety of situations.

3.1. Predicting the Effect of J-modulation with Numerical Simulations

3.1.1. Case of Weak Coupling

To evaluate the ability to predict J-modulation, the UF CT-COSY sequence was simulated for different t_{mix} increments with steps of 5 ms. All simulations were performed with the Spinach package, which was adapted to include the simulation of spatial encoding schemes. A fixed spatial encoding duration of $TE = 30$ ms was used for all simulations, which corresponded to typical experimental parameters in UF CT-COSY. This series of simulations was performed on a small molecule, Ala, which provided a weak coupled system A_3X with a scalar coupling constant of 7.24 Hz (Figure 2 A and B). For each increment of t_{mix}, the peak volumes were measured by integration on the simulated spectra. The same procedure was performed experimentally, and then the results were compared with the simulated data and analytical expressions established in the previous section (Figure 2 C–F).

To take transverse relaxation into account, both simulated data and analytical expressions were multiplied by a pure exponential factor with a decay constant of τ. The latter was estimated experimentally from the signal decay observed as a function of t_{mix} for a peak without J-modulation, that is, the singlet of Cho, which was added to all samples described herein and used as an internal reference for relaxation effects. The τ decay constant was estimated at 220 ms from a series of experiments in which t_{mix} ranged from 0 to 1000 ms. In this study, we assume that all small molecules studied have similar τ decay constants; this assumption is supported a posteriori by the good match between analytical, simulated, and experimental results. The effect of J-modulation predicted by the analytical expressions and numerical simulations matches very well with the experimental data (Figure 2 C–F). The only slight difference is observed for the XX peak, due to a small overlap of the experimental peak with the singlet of the internal relaxation reference (Cho). Also noticeable is the asymmetric evolution of peak intensities for symmetric signals on each side of the diagonal; this effect can be expected because such signals undergo different J-modulation effects. These results highlight the efficiency of our simulation platform for predicting UF spectra of small molecules. Moreover, these curves show that the effect of J-modulation is highly peak dependent, even in a simple case such as Ala.

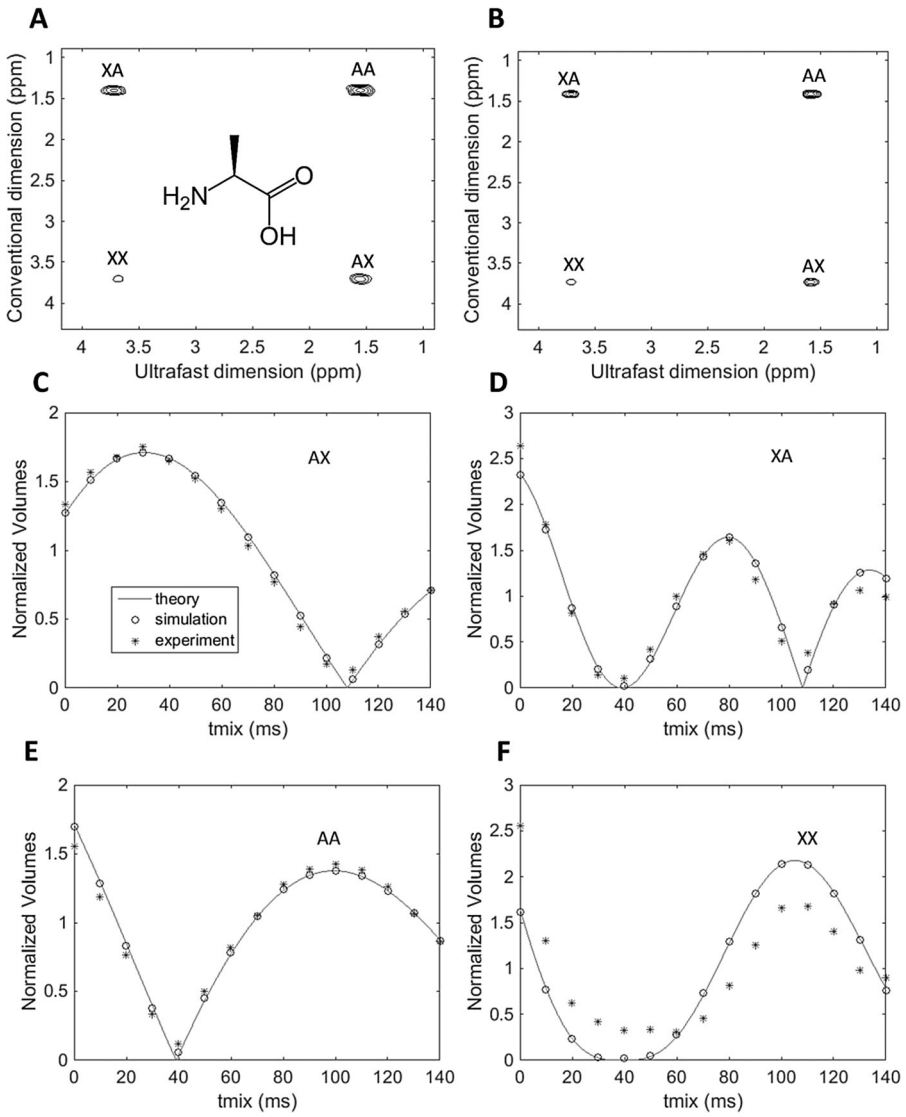

Figure 2. The J-modulation effects in a weakly coupled spin system (Ala). UF CT-COSY spectra obtained experimentally (A) and from Spinach numerical simulations (B) were processed and integrated in the same way. The analytical expressions of J-modulation (solid lines) were compared with results from numerical simulations (circles) and experimental data (crosses). *TE* was set to 30 ms. J-modulation was studied as a function of t_{mix} for the cross-peaks AX (C) and XA (D), and for the diagonal peaks AA (E) and XX (F). All curves were normalized to their mean value.

3.1.2. Case of Strong Coupling

Although the analytical expressions of J-modulation are suitable for the prediction of the optimal t_{mix} in the case of a weakly coupled A_3X spin system, these expressions are no longer valid in the case of strongly coupled spin systems. In this context, numerical simulations are essential to analyze J-modulation. Herein, we evaluated the ability to predict the optimal t_{mix} in such cases with Tau and His samples, which provide strongly coupled A_2B_2 and ABX (geminal coupling) spins systems, respectively (Figure 3 A–F).

As for the Ala sample, transverse relaxation was taken into account with a τ decay constant of 220 ms. A noticeable feature of these spectra is the excellent match between experimental and simulated spectral patterns. The effect of J-modulation is shown for the circled peaks in Figure 3. A good match is obtained for Tau (Figure 3 G), whereas in the case of His the match is only qualitative (Figure 3 H). The discrepancies between simulation and experiment can be explained by the difficulty in accurately determining the actual chemical shifts—used as input values in the simulations—in the presence of second-order effects. Nevertheless, the numerical simulation platform remains efficient enough to predict the local maxima. Overall, even for strongly coupled spin systems, the numerical simulations performed through the Spinach package appear to be a relevant tool to optimize J-modulation for complex spin systems.

3.2. Optimization Strategies and Applications

3.2.1. Best Compromise Strategy

Understanding and predicting the effects of J-modulation can prevent unnecessary sensitivity losses. However, optimization for real-life samples containing different spin systems (either from the same compound or from different molecules) is not straightforward. The first approach consists of choosing the best compromise between different spin systems; an approach that is well suited to spectra of complex mixtures. Let us consider, as an example, the quantification of metabolites inside a mixture, a domain in which UF CT-COSY is recognized to be a powerful tool.[22] We focus herein on the detection of Ala, Lac, Thr, and Tau. Each of these metabolites is usually quantified, relying on a calibration procedure, through one well-resolved cross-peak: Ala (1.47, 3.78) ppm, Lac (1.32, 4.10) ppm, Thr (1.33, 4.26) ppm, and Tau (3.26, 3.42) ppm (Figure 4 B).

Here, the best approach consists of avoiding situations in which some peaks are missing, whereas others have a maximum intensity under the influence of J-modulation effects. On the contrary, a situation in which all signals of interest have a similar response is far more preferable; the limiting factor is the peak with the lowest SNR. Simulating the intensity of the cross-peaks as a function of t_{mix} can help with choosing a compromise value to average the effects of J-modulation. Fig-

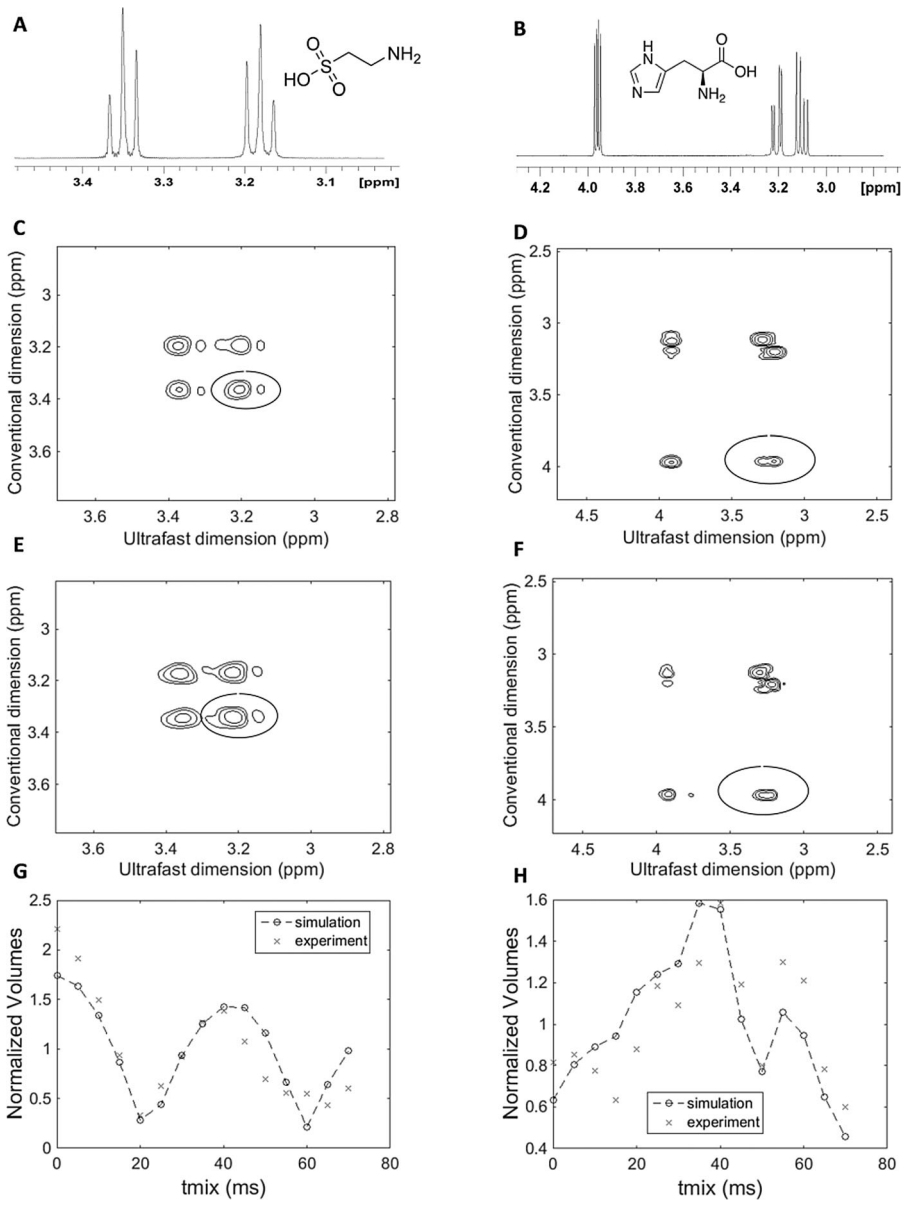

Figure 3. 1D ^{1}H spectra of Tau (A) and His (B) showing strong second-order coupling effects. Simulated CT phase-modulated UF CT-COSY spectra of the A_2B_2 spin system from Tau (C), and the ABX spin system from His (D) performed with the Spinach package. *TE* was set to 30 ms in all cases. Experimental CT phase-modulated UF CT-COSY spectra of Tau (E) and His (F). Integral of the simulated versus experimental signals as a function of t_{mix} for the circled cross-peaks of Tau (G) and His (H).

ure 4A shows these curves for the system described above, obtained on a series of 15 simulated spectra with t_{mix} values ranging from 0 to 140 ms. To predict the local maxima more accurately, data from numerical simulations were multiplied by a pure exponential decay with a τ decay constant of 220 ms. From these curves, an optimum t_{mix} of 20 ms can be chosen, leading to a sensitivity improvement of about 20% for Lac, Thr, and Ala cross-peaks, whereas the SNR of the Tau peak is decreased to match those of the other metabolites (Figure 4B and C). This sensitivity optimization requires knowing the characteristics of the detected compounds accurately, which is usually the case in a quantification issue. Regarding quantitative applications, it should be noted that the coefficient of proportionality between peak volumes and concentrations will remain peak dependent in most cases; hence, the need to rely on a calibration protocol because this is the case in almost all quantitative 2D NMR spectroscopy experiments.[23]

3.2.2. Recording Spectra without Missing Signals

Although this first example requires optimizing the sensitivity of one specific peak for each spin system, other common situations, such as structure eluci-

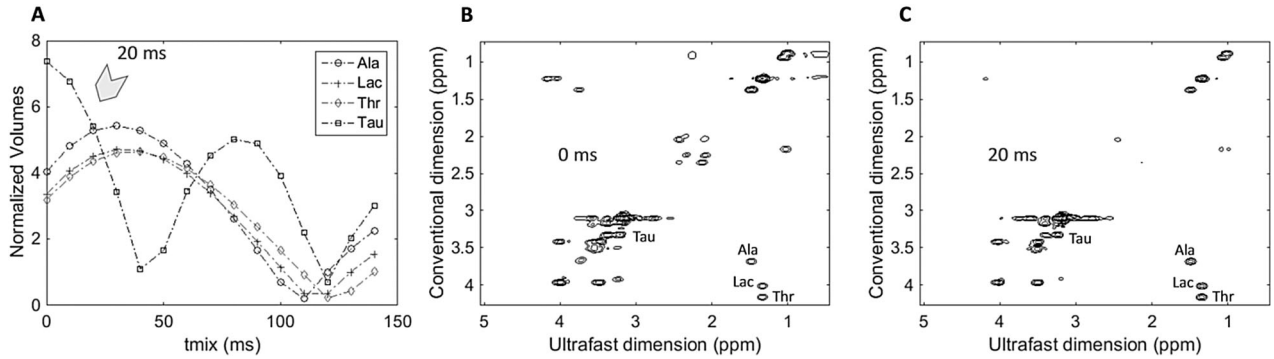

Figure 4. Calculated signals as a function of t_{mix} (with $TE = 30$ ms) for the cross-peaks of interest from Ala, Lac, Thr, and Tau. A compromise is found at $t_{mix} = 20$ ms (A). Experimental CT phase-modulated UF CT-COSY spectra of a 50 mmol L^{-1} mixture of metabolites in D_2O, recorded in a single-scan at 500 MHz, with a cryoprobe for t_{mix} values at 0 (B) and 20 ms (C)

dation, require the observation of all peaks arising from a given molecule. Unfortunately, as mentioned above, J-modulation effects can lead to missing peaks in the 2D spectra. This phenomenon is clearly illustrated on the case of ferulic acid (Figure 5 A), which is a small molecule that shows a variety of coupling patterns. Under non-optimized experimental conditions, two diagonal peaks are missing, CC at (7.16, 7.16) ppm and DD at (6.89, 6.89) ppm, whereas two symmetric cross-peaks, AE (6.40, 7.63) and EA (7.63, 6.40) ppm, show very low intensities (Figure 5 C). These occasional missing peaks become a tricky issue to check or elucidate a molecular structure, which makes it difficult to set up the UF CT experiments as routine sequences. Averaging the effect of J-modulation on all spin systems of interest forms an appealing solution to avoid these missing peaks. Because the sensitivity issues of UF experiments often require the accumulation of a few scans, adding several spectra recorded with incremented t_{mix} values is a convenient way of achieving this in a reasonable time. This multiscan approach was evaluated on the same sample of ferulic acid by adding a series of nine spectra with t_{mix} values ranging from 0 to 40 ms. The resulting spectrum (Figure 5 D), recorded in 46.13 s, contains all expected peaks, which shows the efficiency of this approach. This straightforward method has the advantage of being applicable to unknown samples.

3.2.3. Enhancement of Cross-Peak Intensities for Multiple Spin Systems

While achieving the detection of all expected peaks, the multiscan approach does not maximize peak intensity because it results from signal averaging of the J-modulation effects. Nevertheless, several applications, such as reaction monitoring, require maximizing the intensity of the cross-peaks, and being able to achieve this in a single scan would be particularly appealing. This requires, however, the simultaneous optimization of J-modulation effects for different spin systems. To achieve this goal, we propose a new excitation block in which the 90° hard pulse is replaced by spectrally selective pulses followed by delays to excite each spin system of the sample successively and independently (Figure 5 E). These selective pulses are separated by suitably chosen delays, which are calculated so that each spin system spends an optimal time in the transverse plane to optimize the effect of J-modulation. The optimum delay can be predicted from the calculated (or simulated) J-modulation curves (Figure 5 F). This single-scan approach was applied to the ferulic acid sample characterized by two different spin systems (Figure 5 A). The corresponding spin systems have very different *J*-coupling constants (16.0 Hz for AE and 8.1 Hz for CD). Thanks to a prediction of the J-modulation for each cross-peak, the interpulse delay can

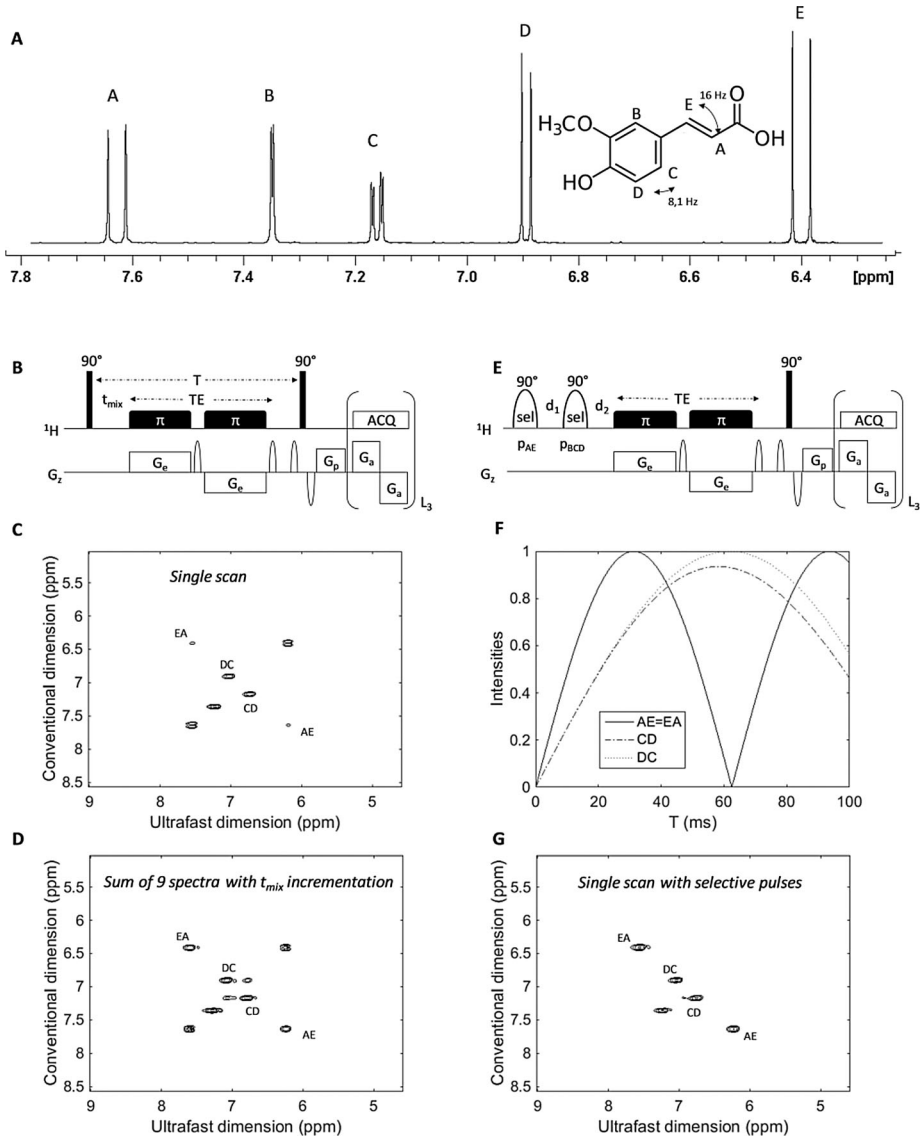

Figure 5. A) 1D ^{1}H NMR spectrum of a 207 mmol L^{-1} ferulic acid sample in [D_6]acetone. The molecular structure is shown with the corresponding *J*-coupling constants. Pulse sequence for CT phase-modulated UF-COSY (B), and the corresponding spectrum of ferulic acid recorded in 1 scan with a t_{mix} of 30 ms (C), and by adding 9 spectra acquired with a t_{mix} incrementation of 5 ms per scan from 0 to 40 ms (D), with $TE = 30$ ms. E) Pulse sequence for CT phase-modulated UF CT-COSY, including a new excitation block based on spectrally selective pulses. F) Calculated J-modulation as a function of *T*, that is, the total time spent in the transverse plan, for the cross-peaks of ferulic acid. UF CT-COSY spectrum obtained with the pulse sequence shown in E) by using the new excitation block (G).

be adjusted, so that each spin system reaches the maximum of its J-modulation curve in the same experiment (Figure 5F). In this example, p_{AE} and p_{BCD} are the durations of the selective pulses that excite spins A–E and B–C–D, respectively. Notably, the pulse exciting A and E has to be polychromatic to excite two different regions at the same time. The interpulse delays d_1 and d_2 can be computed by relying on Equation (12), in which T_{AE} and T_{BCD} represent the total time spent in the transverse plane for spin systems AE and BCD, respectively.

$$\begin{cases} T_{AE} = \frac{p_{AE}}{2} + d_1 + p_{BCD} + d_2 + TE \\ T_{BCD} = \frac{p_{BCD}}{2} + d_2 + TE \end{cases} \quad (12)$$

By relying on Equation (12) and on the calculated J-modulation curves, an UF CT-COSY spectrum with this excitation block was recorded on the ferulic acid sample with $d_1 = 17.5$ ms and $d_2 = 27.8$ ms. The selective pulses had a Gaussian shape with a duration of $p_{AE} = 17.91$ ms for the first one and $p_{BCD} = 7.15$ ms for the second one. The resulting spectrum (Figure 5G) clearly shows the high cross-peak intensity reached for all correlation peaks within a single scan and also results in a strong decrease in the diagonal peaks. This approach requires fine-tuning of the pulse sequence parameters and is therefore suitable for the study of spin systems that are a priori known.

Due to the use of selective pulses, it is also limited by the position of peaks in the 1D spectrum, but polychromatic pulses make it possible to excite several distinct spectral regions simultaneously. Therefore, this approach could be useful when the intensity of targeted cross-peaks needs to be optimized, such as in the monitoring of real-time dynamic phenomena that generally focus on targeted cross-peaks.

4. Conclusions

We highlighted the significant role of J-modulation as a potential source of sensitivity losses in the case of UF CT experiments, and demonstrated how understanding J-modulation effects leads to significant sensitivity recovery in a variety of situations. The combination of theoretical description and numerical simulations showed the possibility of predicting the J-modulation effects for several spin systems, even those that were strongly coupled. Based on this prediction, several single- or multiscan strategies were designed to optimize the peak intensity in UF CT-COSY spectra. The optimal strategy depended on targeted applications, and the potential and drawbacks of different approaches were discussed, so that a user could choose the optimal approach for a given situation. We hope that these tools will help users of UF NMR spectroscopy to tune the sensitivity of their experiments for a wide range of applications.

Acknowledgements

We warmly thank Prof. Malcolm H. Levitt (University of Southampton) for fruitful discussions. Funding from the Région Pays de la Loire (Grant RésoNantes) is also acknowledged.

Keywords: computational chemistry · J-modulation · natural products · NMR spectroscopy · ultrafast spectroscopy

[1] a) W. P. Aue, E. Bartholdi, R. R. Ernst, *J. Chem. Phys.* **1976**, *64*, 2229–2246; b) J. Jeener, lecture presented at *Ampere International Summer School II*, Basko Polje, Yugoslavia, **1971**.
[2] G. A. Morris, *J. Magn. Reson.* **1992**, *100*, 316–328.
[3] P. Schanda, B. Brutscher, *J. Am. Chem. Soc.* **2005**, *127*, 8014–8015.
[4] P. Schanda, H. Van Melckebeke, B. Brutscher, *J. Am. Chem. Soc.* **2006**, *128*, 9042–9043.
[5] E. Kupče, R. Freeman, *Magn. Reson. Chem.* **2007**, *45*, 2–4.
[6] a) A. S. Stern, K.-B. Li, J. C. Hoch, *J. Am. Chem. Soc.* **2002**, *124*, 1982–1993; b) H. Barkhuijsen, R. De Beer, W. M. M. J. Bovée, D. Van Ormondt, *J. Magn. Reson.* **1985**, *61*, 465–481; c) J. C. Hoch, *J. Magn. Reson.* **1985**, *64*, 436–440.
[7] a) E. Kupče, R. Freeman, *J. Magn. Reson.* **2003**, *162*, 158–165; b) E. Kupče, R. Freeman, *J. Magn. Reson.* **2003**, *162*, 300–310.
[8] a) L. Frydman, T. Scherf, A. Lupulescu, *Proc. Natl. Acad. Sci. USA* **2002**, *99*, 15858–15862; b) L. Frydman, A. Lupulescu, T. Scherf, *J. Am. Chem. Soc.* **2003**, *125*, 9204–9217.
[9] a) P. Mansfield, *J. Phys. C* **1977**, *10*, 55–58; b) A. Tal, L. Frydman, *Prog. Nucl. Magn. Reson. Spectrosc.* **2010**, *57*, 241–292.
[10] Y. Shrot, L. Frydman, *J. Chem. Phys.* **2008**, *128*, 052209.
[11] P. Pelupessy, *J. Am. Chem. Soc.* **2003**, *125*, 12345–12350.
[12] P. Giraudeau, L. Frydman, *Annu. Rev. Anal. Chem.* **2014**, *7*, 129–161.
[13] a) Y. Shrot, L. Frydman, *J. Chem. Phys.* **2009**, *131*, 224516; b) P. Pelupessy, L. Duma, G. Bodenhausen, *J. Magn. Reson.* **2008**, *194*, 169–174.
[14] a) Z. Wei, L. Lin, Q. Ye, J. Li, S. Cai, Z. Chen, *J. Chem. Phys.* **2015**, *143*, 024201; b) P. Giraudeau, S. Akoka, *J. Magn. Reson.* **2010**, *205*, 171–176.
[15] a) Y. Shrot, L. Frydman, *J. Chem. Phys.* **2008**, *128*, 164513; b) P. Giraudeau, S. Akoka, *J. Magn. Reson.* **2008**, *192*, 151–158; c) L. Rouger, D. Loquet, S. Massou, S. Akoka, P. Giraudeau, *ChemPhysChem* **2012**, *13*, 4124–4127; d) P. Giraudeau, S. Akoka, *J. Magn. Reson.* **2008**, *190*, 339–345.
[16] a) M. E. Girvin, *J. Magn. Reson. Ser. A* **1994**, *108*, 99–102; b) D. Mayer, W. Dreher, D. Leibfritz, *Magn. Reson. Med.* **2000**, *44*, 23–28; c) H. Watanabe, N. Takaya, F. Mitsumori, *NMR Biomed.* **2008**, *21*, 518–526.
[17] C. Wu, M. Zhao, S. Cai, Y. Lin, Z. Chen, *J. Magn. Reson.* **2010**, *204*, 82–90.
[18] H. J. Hogben, M. Krzystyniak, G. T. P. Charnock, P. J. Hore, I. Kuprov, *J. Magn. Reson.* **2011**, *208*, 179–194.
[19] B. Fornberg, *Math. Comput.* **1988**, *51*, 699–706.
[20] R. R. Ernst, G. Bodenhausen, A. Wokaun, *Principles of Nuclear Magnetic Resonance in One and Two Dimensions*, Clarendon, Oxford, **1987**.
[21] a) H. J. Hogben, P. J. Hore, I. Kuprov, *J. Chem. Phys.* **2010**, *132*, 174011; b) I. Kuprov, *J. Magn. Reson.* **2008**, *195*, 45–51.
[22] T. Jézéquel, C. Deborde, M. Maucourt, V. Zhendre, A. Moing, P. Giraudeau, *Metabolomics* **2015**, DOI: 10.1007/s11306-015-0780-0.
[23] P. Giraudeau, *Magn. Reson. Chem.* **2014**, *52*, 259–272.

Manuscript received: June 29, 2015
Final Article published: ■■ ▮▮, 2015

ARTICLES

Sensitive response: The impact of J-modulation on ultrafast 2D NMR spectroscopy experiments is investigated through numerical simulations (see figure). Optimization strategies are designed to maximize sensitivity in ultrafast COSY spectra of multiple spin systems.

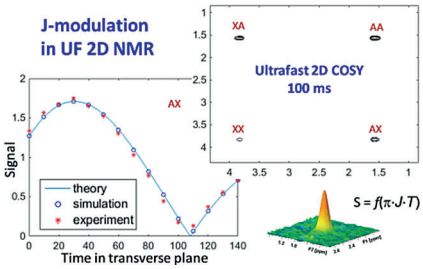

B. Gouilleux, L. Rouger, B. Charrier, I. Kuprov, S. Akoka, J.-N. Dumez, P. Giraudeau**

■■ – ■■

Understanding J-Modulation during Spatial Encoding for Sensitivity-Optimized Ultrafast NMR Spectroscopy

These are not the final page numbers! ↗↗